Polarization-selective vortex-core switching by tailored orthogonal Gaussian-pulse currents

Young-Sang Yu,[1] Ki-Suk Lee,[1] Hyunsung Jung,[1] Youn-Seok Choi,[1] Myoung-Woo Yoo,[1] Dong-Soo Han,[1]
Mi-Young Im,[2] Peter Fischer,[2] and Sang-Koog Kim[1,2,*]

[1]*National Creative Research Initiative Center for Spin Dynamics and Spin-Wave Devices, and Nanospinics Laboratory, Research Institute of Advanced Materials, Department of Materials Science and Engineering, Seoul National University, Seoul 151-744, South Korea*
[2]*Center for X-ray Optics, Lawrence Berkeley National Laboratory, Berkeley CA 94720, USA*
(Received 13 October 2010; revised manuscript received 11 March 2011; published 17 May 2011)

We experimentally demonstrate low-power-consumption vortex-core switching in magnetic nanodisks using tailored rotating magnetic fields produced with orthogonal and unipolar Gaussian-pulse currents. The optimal width of the orthogonal pulses and their time delay are found, from analytical and micromagnetic numerical calculations, to be determined only by the angular eigenfrequency ω_D for a given vortex-state disk of polarization p, such that $\sigma = 1/\omega_D$ and $\Delta t = \frac{\pi}{2} p/\omega_D$. The estimated optimal pulse parameters are in good agreement with the experimental results. This work lays a foundation for energy-efficient information recording in vortex-core cross-point architecture.

PACS number(s): 75.40.Gb, 75.40.Mg, 75.60.Jk

I. INTRODUCTION

Magnetic vortices in patterned magnetic dots are very promising candidates for information storage applications, owing to both the energetically stable twofold ground state of their core magnetization[1–5] and the reliability of their core-switching dynamics, as explored thus far.[6–10] Numerous experimental, analytical, and micromagnetic numerical studies have revealed that low-power-driven vortex-core switching in magnetic nanodots can be simply achieved by application not only of in-plane alternating[6] or rotating magnetic fields[11] or spin-polarized currents,[12] but also their pulse forms.[7,8,13–15] Ever since these studies, the fundamentals of ultrafast vortex-core switching dynamics, including their mechanism,[6–10] physical origin,[12,16] and criterion[10,12,17–19] have been subjects of intense research. However, low-power information writing using orthogonally crossed electrodes available in the basic cross-point architecture, an important and very challenging goal, has not yet been demonstrated.

We experimentally demonstrated polarization-selective vortex-core switching using rotating magnetic fields, achieved using orthogonal and unipolar Gaussian-pulse currents. In order to achieve energy-efficient switching using those simple electrodes, we analytically and numerically optimized the width of the orthogonal pulses and their time delay based on Thiele's analytical approach. Using the optimal values, we then successfully demonstrated low-power-driven vortex-core switching in experiments.

II. CONCEPTS OF IDEAL AND PULSE-TYPE ROTATING FIELDS

In our earlier works, we proposed a unique and novel method whereby circular-rotating magnetic fields are utilized for efficient manipulation of polarization-selective vortex-core reversals.[5,18,20] Ideal single-harmonic circular-rotating fields can be expressed as the vector sum of two linearly oscillating harmonic fields, as shown in Fig. 1, and mathematically as $\mathbf{H}_{CCW} = H_0 \cos(\omega_\mathbf{H} t)\hat{\mathbf{x}} + H_0 \sin(\omega_\mathbf{H} t)\hat{\mathbf{y}}$ and $\mathbf{H}_{CW} = H_0 \cos(\omega_\mathbf{H} t)\hat{\mathbf{x}} - H_0 \sin(\omega_\mathbf{H} t)\hat{\mathbf{y}}$. Such a type of magnetic field rotates either counterclockwise (CCW) or clockwise (CW) on

the film plane with a constant magnetic field strength H_0 and a single-harmonic frequency $\omega_\mathbf{H}$ (Fig. 1). It has been reported that the CCW (CW) rotating field can switch only the upward (downward) core to its reversed orientation with the lowest H_0 value when the field frequency $\omega_\mathbf{H}$ is tuned to the vortex angular eigenfrequency ω_D.[5,11,18] However, such ideal rotating fields are not readily available in real devices.

Our approach in the present work is thus to use, for efficient vortex-core switching, tailored special fields achieved with unipolar Gaussian-pulse currents flowing along two orthogonal electrodes;[11] a cross-type electrode comprised of two striplines orthogonally arranged, as shown in Fig. 2(a). The simplicity of this design builds upon already existing actual memory devices based on the cross-point architecture. Gaussian-shape current pulses can be characterized simply by the pulse width σ and the height I_0. Oersted fields are generated around both current paths. The local fields at the cross point of the two orthogonal electrodes vary in their strength and direction with time and space on the film plane, yielding certain types of rotating field. The rotation sense of the resultant rotating fields varies primarily with delay time Δt between the two orthogonal currents [see Figs. 2(b) and 2(c)]. For example, $\Delta t = 0$ indicates certain linear fields, but $\Delta t < 0$ and $\Delta t > 0$ represent the CW and CCW sense of the rotating fields, respectively. The dominant frequency can be determined according to σ. Thus, a certain combination of the Δt and σ values represents a special rotating field, named the pulse-type rotating field in order to distinguish it from the ideal single-harmonic circular-rotating field mentioned earlier.

III. OPTIMIZING THE CURRENT PULSE PARAMETERS

A. Analytical derivations

In order to find the optimal values of the pulse parameters by which vortex-core switching events can be achieved with the lowest value of H_0, we employed analytical derivations and numerical calculations of the vortex-core motions in response to different pulse parameters, based on Thiele's equation.[21]

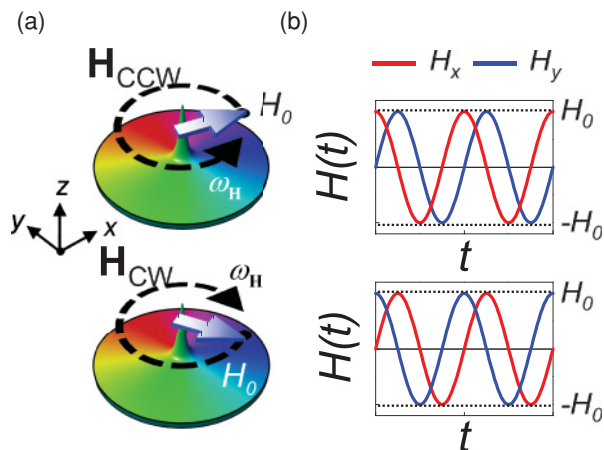Rotating magnetic fields obtained from the aforementioned orthogonal unipolar Gaussian-pulse

FIG. 1. (Color online) (a) Schematic illustration of ideal counterclockwise (CCW) and clockwise (CW) circular-rotating magnetic fields. (b) Time-varying oscillating magnetic fields produced by two orthogonal alternating currents.

currents can be expressed mathematically as $\mathbf{H}_{\text{Rot}} = \mathbf{H}_x + \mathbf{H}_y$ with $\mathbf{H}_x = H_{x0} \exp[-t^2/(2\sigma^2)]\hat{\mathbf{x}}$ and $\mathbf{H}_y = H_{y0} \exp[-(t - \Delta t)^2/(2\sigma^2)]\hat{\mathbf{y}}$ as seen in Fig. 3(a). Such pulse-type rotating fields, in contrast to the corresponding ideal circular-rotating fields, have time- and space-varying field strengths [see Fig. 2(c)] as well as many different harmonic frequencies along with a certain frequency profile. This type of field can be considered to be a mixture of ideal circular-rotating fields, each of which has a different constant field strength and different single-harmonic frequency, as shown in Figs. 3(b) and 3(c). In reference to the circular-rotating-frame basis and complex variables, an ideal circular-rotating field of strength h_0, phase ϕ, and frequency ω_h can be expressed mathematically as $\tilde{h}e^{i\omega_h t} = h_0 e^{i\phi} e^{i\omega_h t} = h_0 \cos(\omega_h t + \phi) + i h_0 \sin(\omega_h t + \phi)$. Here $\omega_h > 0$ and $\omega_h < 0$ correspond to the CCW and CW rotation sense, respectively. The power spectra of individual harmonics vary markedly with the values of Δt and σ, as shown in Figs. 3(b) and 3(c), respectively, and as calculated from $\tilde{h}(\omega_h) = \frac{1}{\sqrt{2\pi}} \int_{-\infty}^{\infty} \tilde{H}(t)e^{-i\omega_h t}dt$ with $\tilde{H} = H_{x0} \exp[-t^2/(2\sigma^2)] + i H_{y0} \exp[-(t - \Delta t)^2/(2\sigma^2)]$ and $H_{x0} = H_{y0} = H_0$.

To derive explicit analytical equations, we start with a susceptibility tensor[20] for vortex-core motions driven by linearly polarized harmonic fields: $\hat{\chi}_{X,L}(\omega_{\mathbf{H}}) = \mathbf{X}_{0,L}/\mathbf{H}_{0,L}$, with the vortex-core position vector $\mathbf{X} = \mathbf{X}_{0,L} \exp(-i\omega_{\mathbf{H}}t)$, the harmonic oscillating field $\mathbf{H} = \mathbf{H}_{0,L} \exp(-i\omega_{\mathbf{H}}t)$, and the angular frequency $\omega_{\mathbf{H}}$ (>0). The equation of $\hat{\chi}_{X,L}(\omega_{\mathbf{H}}) = \mathbf{X}_{0,L}/\mathbf{H}_{0,L}$ can be rewritten, in matrix form, as

$$\begin{pmatrix} X_{0,x} \\ X_{0,y} \end{pmatrix} = \frac{\mu}{(i\omega_{\mathbf{H}}D + \kappa)^2 - (\omega_{\mathbf{H}}G)^2}$$
$$\times \begin{bmatrix} -i\omega_{\mathbf{H}}G & -i\omega_{\mathbf{H}}D - \kappa \\ i\omega_{\mathbf{H}}D + \kappa & -i\omega_{\mathbf{H}}G \end{bmatrix} \begin{pmatrix} H_{0,x} \\ H_{0,y} \end{pmatrix}, \quad (1)$$

where $\mathbf{X}_{0,L} = X_{0x}\hat{\mathbf{x}} + X_{0y}\hat{\mathbf{y}}$ and $\mathbf{H}_{0,L} = H_{0x}\hat{\mathbf{x}} + H_{0y}\hat{\mathbf{y}}$, along with $\mu = \pi R L M_s \xi C$ for the circular disk with radius R, thickness L, and the saturation magnetization M_s, the chi-
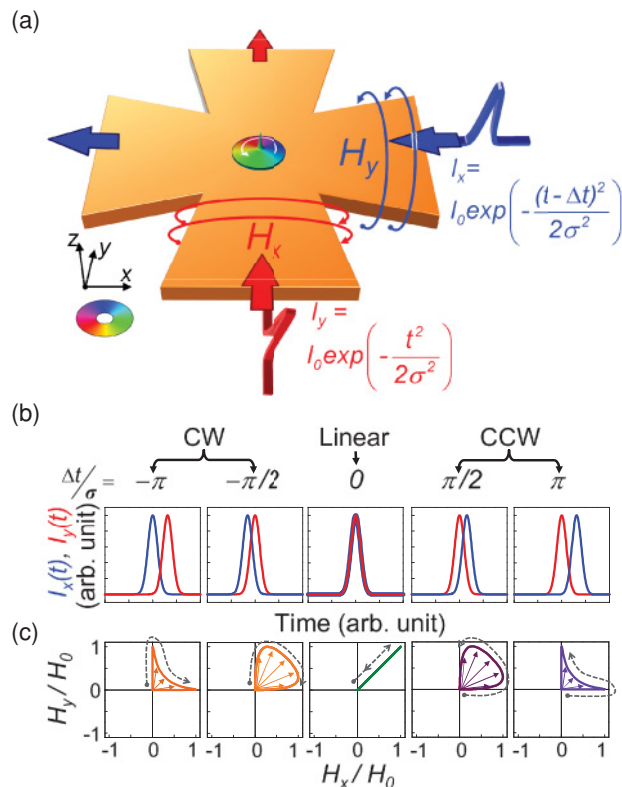

FIG. 2. (Color online) (a) Schematic illustration of sample consisting of single Py disk and two-crossed-stripline electrode. The color and height of the indicated initial vortex state indicate the local in-plane and out-of-plane magnetization components, respectively. (b) Two Gaussian-pulse currents flowing along x [blue (dark gray)] and y [red (medium gray)] axes with indicated different $\Delta t/\sigma$ values. (c) Pulse-type rotating fields at intersection of two striplines. The dotted arrows indicate the rotation sense of the resultant fields on the plane.

rality of vortex C ($C = +1$ for the CCW in-plane curling magnetization direction and $C = -1$ for the CW direction), and $\xi = 2/3$ for the "side-charge-free" model, the stiffness coefficient κ, the gyrovector constant G, and the damping constant D.[22] The vortex-core displacement from the center position in response to a single-harmonic circular-rotating field, $\tilde{h}e^{i\omega_h t}$ can thus be expressed simply as $\tilde{X} = \chi_{\omega_h}\tilde{h}$, with the complex-variable position vector $\tilde{X}e^{i\omega_h t} \equiv X_x + i X_y$, the single-harmonic circular-rotating field $\tilde{h}e^{i\omega_h t} = h_x + i h_y$ and the complex susceptibility $\chi_{\omega_h} = i\mu/(\kappa - \omega_h G - i\omega_h D)$.[18] Finally, integrating all of the vortex-core motion responses to individual harmonic fields, expressed mathematically as $\tilde{X}(t) = \frac{1}{\sqrt{2\pi}} \int_{-\infty}^{\infty} \chi_{\omega_h}\tilde{h}(\omega_h)e^{i\omega_h t}d\omega_h$, gives rise to resultant positions of dynamic vortex-core motion.

Figure 4 shows the results of the numerical calculations of $|\chi_{\omega_h}|$ and $|\chi_{\omega_h}\tilde{h}(\omega_h)|$ as a function of the reduced parameter of ω_h/ω_d for the indicated $\Delta t/\sigma$ values. The absolute value of $\tilde{X}(\omega_h) = \chi_{\omega_h}\tilde{h}(\omega_h)$ represents the steady-state radius of the corresponding vortex-core displacement at each harmonic frequency. Given the fact that vortex-core gyrations arise resonantly at $\omega_h = \omega_d$ (where $\omega_d = p\omega_D$), the gyration-assisted low-power-driven switching can be maximized with $\omega_h = \omega_d$, where
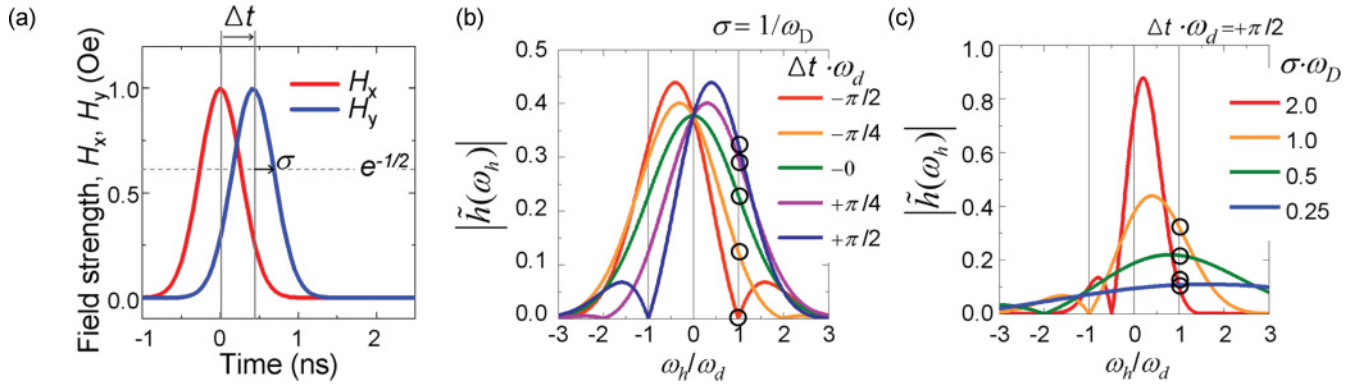
FIG. 3. (Color online) (a) Two pulse fields produced by the corresponding Gaussian-pulse currents, along with given Δt and σ values. Power spectra versus harmonic frequency for pulse-type rotating fields resulting from the vector sum of two orthogonal fields for indicated different values of $\Delta t/\sigma$ (at $\sigma = 1/\omega_D$) in (b) and $\sigma \omega_D$ (at $\Delta t \omega_d = +\pi/2$) in (c), where $\omega_d/2\pi = 580$ MHz.

$\omega_D = \kappa|G|/(G^2 + D^2)$ with the same notations defined in Ref. 20. The maximum value of $|\tilde{h}(\omega_h)|$ can be found at $\omega_h = \omega_d$, where $\tilde{h}(\omega_h) = H_0\sigma \exp(-\sigma^2\omega_h^2/2)[1 + i \exp(-i\omega_h\Delta t)]$, and is given as $|\tilde{h}(\omega_d)| = H_0\sigma \exp(-\sigma^2\omega_d^2/2)\sqrt{2 + 2\sin(\omega_d\Delta t)}$. The $|\tilde{h}(\omega_d)|$ at $\omega_h = \omega_d$ varies dramatically with Δt at a constant σ value of $1/\omega_D$ and with σ at a constant Δt value of $\frac{\pi}{2}p/\omega_D$, as shown in Figs. 3(b) and 3(c), respectively. The numerical calculations of $|\tilde{h}(\omega_d)|/H_0 = \sigma \exp(-\sigma^2\omega_d^2/2)\sqrt{2 + 2\sin(\omega_d\Delta t)}$ show the maxima of $|\tilde{h}(\omega_d)|$ at $\sigma = 1/\omega_D$ and $\Delta t = p(2n + \frac{1}{2})\pi/\omega_D$ with $n = 0$, ±1, ±2, ... (see the dashed vertical gray lines in Fig. 5). For large n values, such magnetic fields become close to certain linear Gaussian-pulse fields applied individually along the x or y axis. Note that the optimal pulse parameters are determined only by ω_D for a given vortex of its polarization p. We also emphasize that the dominant frequencies (peaks) in the power spectra of harmonics are not equal to the eigenfrequency at which σ and Δt are optimized to obtain the largest value of $|\tilde{h}(\omega_h = \omega_d)|$.

B. Micromagnetic numerical calculation

The above analytical estimates were also confirmed from micromagnetic simulations for vortex-core motions, responding to different values of σ and Δt, in a Py disk of radius $R = 150$ nm and thickness $L = 20$ nm, for the upward core orientation ($p = +1$). Here, to reduce the computation time, we used a much smaller Py disk than in the experiment. We employed the OOMMF code,[23] which utilizes the Landau-Lifshitz-Gilbert equation of motion of magnetization, $\partial\mathbf{M}/\partial t = -\gamma (\mathbf{M} \times \mathbf{H}_{\text{eff}}) + (\alpha/|\mathbf{M}|) (\mathbf{M} \times \partial\mathbf{M}/\partial t)$ (Ref. 24), with the gyromagnetic ratio γ (2.21×10^5 m/As) and the phenomenological damping constant α (0.01). We set the unit cell size at $2 \times 2 \times 20$ nm^3. The standard Py material parameters used are as follows: the saturation magnetization $M_s = 8.6 \times 10^5$ A/m, the exchange stiffness $A_{\text{ex}} = 1.3 \times 10^{-11}$ J/m, and the magnetocrystalline anisotropy constant $K = 0$. The simulation results (symbols) of the maximum radius of the vortex-core gyrations versus σ (at $\Delta t = 0$) and Δt (at $\sigma = 1/\omega_D$) are shown in Figs. 6(a) and 6(b), respectively. The solid lines indicate the numerical solution of the analytically derived equations. The simulation and analytical calculations agree very well quantitatively. The values of $\sigma = 274.4$ ps and $\Delta t = 431.0$ ps, which were obtained by inserting $\omega_D = 2\pi \times 580$ MHz into the analytical forms of $\sigma = 1/\omega_D$ and $\Delta t = \frac{1}{2}\pi/\omega_D$, are very close to the simulation values of σ (=275 ps) and Δt (=431 ps).

IV. EXPERIMENTAL OBSERVATION

A. Sample preparation

As the next step, we experimentally investigated vortex-core switching events driven by pulse-type rotating fields,
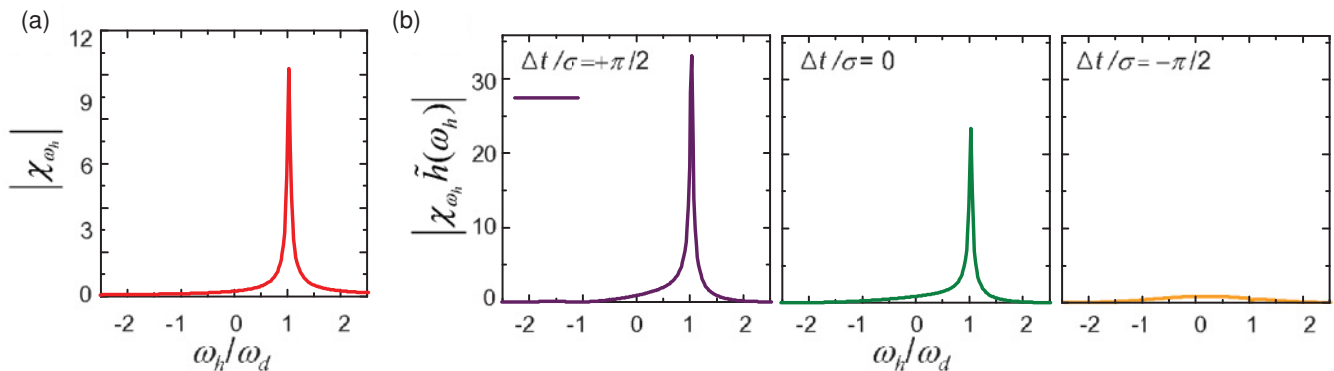

FIG. 4. (Color online) Calculations of (a) $|\chi_{\omega_h}|$ and (b) $|\chi_{\omega_h}\tilde{h}(\omega_h)|$ versus ω_h/ω_d for up-core gyration, in Py disk of $R = 150$ nm and $L = 20$ nm, by pulse-type rotating fields of $\sigma = 274.4$ ps and indicated different values of $\Delta t/\sigma$.
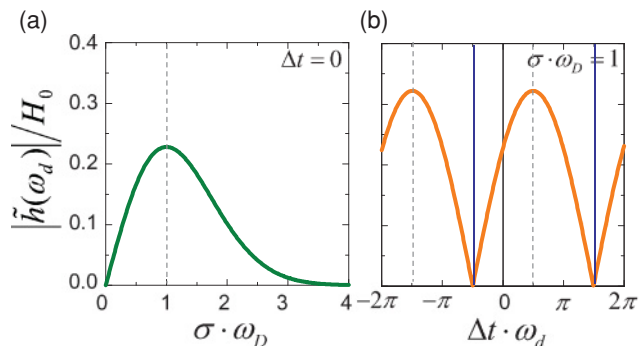
FIG. 5. (Color online) $\left|\tilde{h}(\omega_d)\right|/H_0$ versus $\sigma\omega_D$ at $\Delta t = 0$ in (a) and versus $\Delta t \omega_d$ at $\sigma = 1/\omega_D$ in (b).

using a sample consisting of a Permalloy (Py: $Ni_{80}Fe_{20}$) disk on crossed electrodes, as illustrated in Fig. 2(a). The Py films were deposited by magnetron sputtering under base pressures of $<5 \times 10^{-9}$ Torr. Py disks of radius $R = 2.5$ μm and thickness $L = 70$ nm were patterned by typical e-beam lithography (Jeol, JBX9300FS) and subsequent lift-off processes. Each disk was placed at the intersection of two 50-nm-thick stripline Au electrodes and capped with 2-nm-thick Pd layers (without breaking the vacuum) to prevent oxidation. Such cross-type electrodes similar to those employed in Ref. 11 were patterned by e-beam lithography and subsequent lift-off processes. In order to obtain sufficient soft x-ray transmission through the sample, the electrodes were deposited onto the 200-nm-thick silicon nitride membranes of a 5 mm $\times$ 5 mm window by electron-beam evaporation under base pressures of $<1 \times 10^{-8}$ Torr.

B. Soft x-ray microscopy measurements

Vortex-core switching events were then examined involving the aforementioned pulse-type rotating fields of different values of I_0 (H_0), σ, and Δt. In the present study, the strength H_0 of the fields was estimated directly from I_0 through Ampere's law. By varying the pulse-parameter values, we manipulated the polarization, strength and frequency profiles
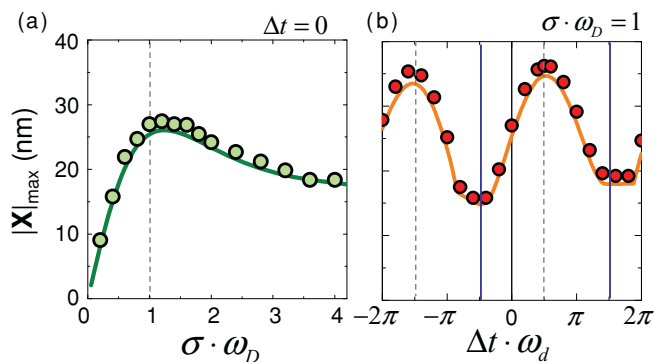

FIG. 6. (Color online) Comparison between analytical calculation (solid lines) and micromagnetic simulation (symbols) for the maximum radius $|X|_{max}$ of gyrotropic motions of upward core orientation ($p = +1$, $\omega_d = \omega_D$) in Py disk of $R = 150$ nm and $L = 20$ nm. $H_0 = 50$ Oe was used in both the simulation and analytical calculations.
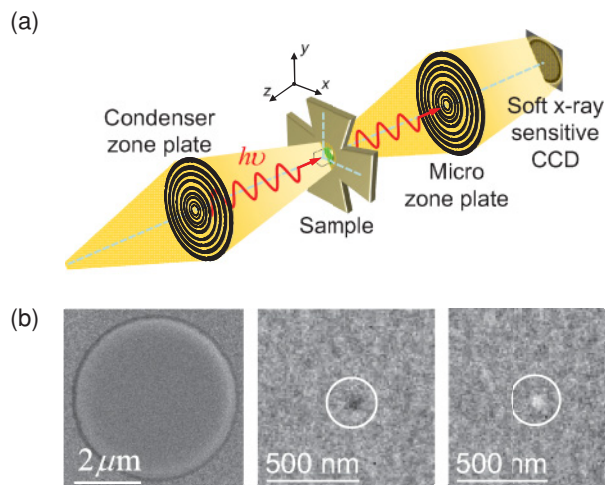

FIG. 7. (Color online) (a) Schematic illustration of our experimental setup for MTXM measurements. The two Fresnel zone plates project a full-field image of the spatial distribution of the local magnetizations onto a soft-x-ray-sensitive CCD camera. In the experiment, the soft x rays were incident normal to the surface of the samples so that the out-of-plane components of the vortex-core magnetizations could be directly monitored. (b) Left: Scanning electron microscope image of single Py disk of radius $R = 2.5$ μm and thickness $L = 70$ nm, placed on two-crossed-stripline Au electrode. The spatial distribution of the local out-of-plane magnetizations around the core regions, for upward (middle) and downward (right) core orientation, before and after switching.

of those fields as shown in Fig. 2(c). In order to directly monitor the out-of-plane magnetizations of the initial core orientations, either upward or downward, we employed high-resolution magnetic transmission soft x-ray microscopy (MTXM) at the Advanced Light Source in Berkeley, California [Fig. 7(a)], which utilizes the x-ray magnetic circular dichroism (XMCD) contrast at the Fe L_3 edge.[25] A scanning electron microscope image of a single Py disk and the representative MTXM images around the core region are shown in Fig. 7(b). The dark and white spots indicate the upward and downward core orientations, respectively, in our experimental setup, before and after a vortex-core switching event. By monitoring the dark and white spots in these experimental XMCD images, we can readily determine whether vortex-core switching events had occurred for a given field pulse.

V. RESULTS

We present some experimental results along with the prediction of the boundary diagrams of vortex-core switching events driven by pulse-type, CCW rotating fields and linear fields. Figure 8 shows the results (open and closed symbols) of three different Py disks of the same $R = 2.5$ μm and $L = 70$ nm dimensions at several different values of σ for the indicated field polarizations, $\Delta t = +2.0$ ns (CCW rotating field) and $\Delta t = 0$ (linear field). In the experiment, the upward-to-downward core switching by the CW rotating fields could not be measured, because much higher field strengths are required for the switching with this type of rotating field, as shown by the orange (light gray) curve.
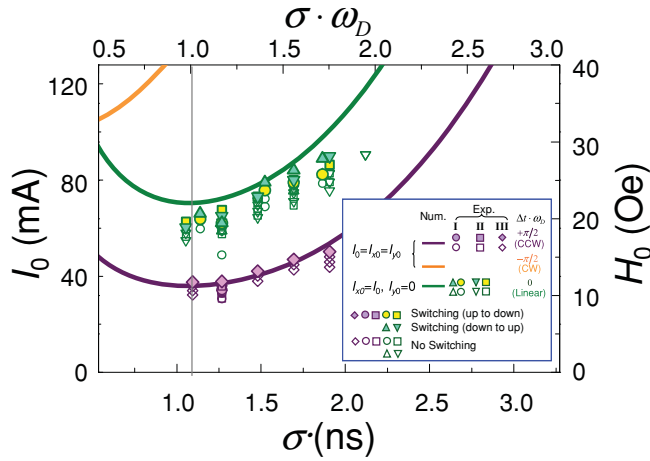
FIG. 8. (Color online) Boundary diagram of vortex-core switching events on plane of σ and I_0 (H_0). The symbols and solid lines indicate the experimental results and analytical calculations, respectively. The experimental results were obtained from three different samples of identical dimensions, as indicated by I, II, and III. The closed and open symbols indicate the occurrence of vortex-core switching and nonswitching events, respectively. The solid vertical line indicates the optimal value of the analytical calculation ($\sigma = 1.09$ ns).

Analytical expressions of the minimum field strengths of the CCW [purple (dark gray)] and CW [orange (light gray)] rotating fields and linear [green (medium gray)] fields were derived on the basis of the linearized Thiele's equation[21] of vortex-core motions and the formulated vortex-core critical velocity.[18] As is apparent in Fig. 8, the analytically calculated boundaries (solid lines) were in general agreement with the experimental ones. The analytically derived σ value (vertical line at $\sigma = 1.09$ ns) is close to the experimental value, $\sigma = 1.27$ ns. This fact seemingly is associated with the difference in the eigenfrequency between the real sample and the model we used for the analytical calculation ($\omega_D/2\pi = 146$ MHz).

Next, we investigated vortex-core switching driven by different values of Δt at the constant optimal σ value of 1.27 ns obtained in the earlier experimental result. Figure 9(a) shows the experimentally determined boundary curves (symbols), the minimum values of I_0 (H_0), which are the so-called threshold values required to switch the initial vortex core of upward (downward) magnetization by the CCW (CW) polarization of pulse-type rotating fields. Each polarization, $\Delta t = 0$, ± 1, ± 2, and ± 3 ns, is illustrated in the inset. For the case of $\Delta t = +2.0$ ns (CCW rotating field), the upward core maintained its initial orientation with $H_0 < 11.0$ Oe (open symbols), and then switched to the downward core orientation with $H_0 \geqslant 11.0$ Oe (closed symbols) [Fig. 9(b), right column]. Even with a further increase to $H_0 = 17.2$ Oe, the once-reversed downward core was not switched back to the initial upward orientation by the CCW rotating field, because the field strengths are much too small for that field to reverse the downward core. By contrast, for the other polarization, $\Delta t = -2.0$ ns (CW rotating field), only the downward core was switched to the upward orientation with $H_0 \geqslant 11.0$ Oe [Fig. 9(b), left column]. For the other rotating fields (i.e., $\Delta t = \pm 1$ and ± 3 ns) the same switching behaviors were
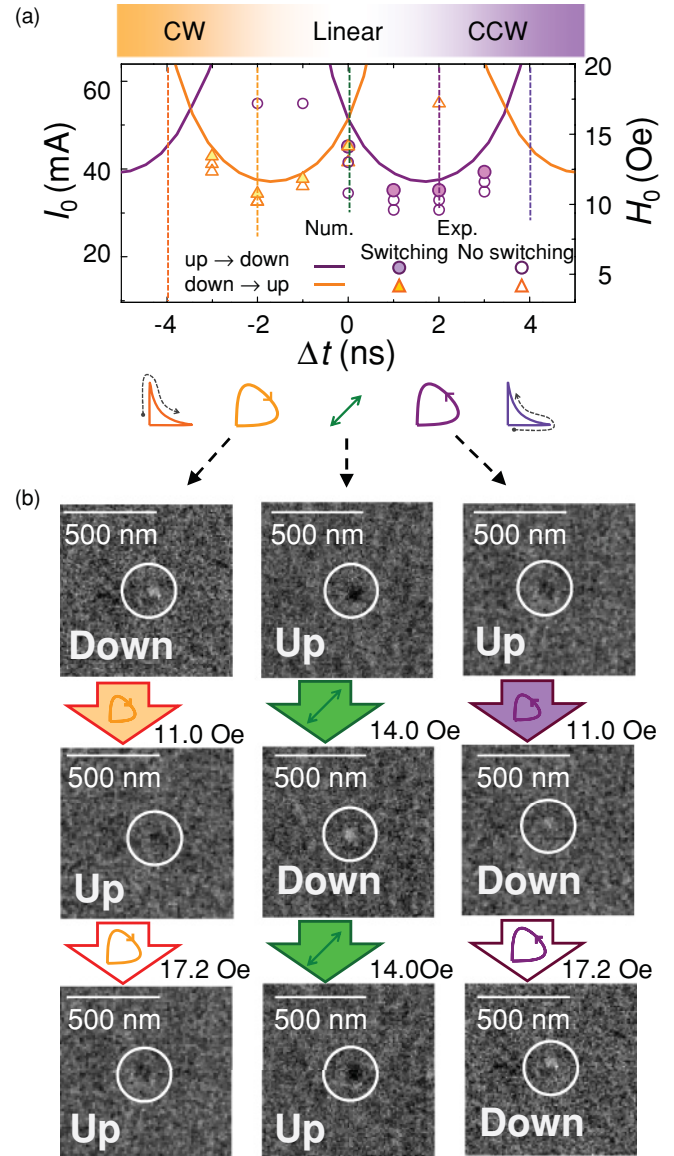

FIG. 9. (Color online) Vortex-core switching diagram on Δt–I_0 (H_0) plane. (a) Boundary diagram of vortex-core switching events, experimentally observed with applications of two orthogonal and unipolar Gaussian-pulse currents of varying I_0 (H_0) at different polarizations $\Delta t = 0$, ± 1, ± 2, and ± 3 ns, with the optimized value of $\sigma = 1.27$ ns. The vertical dashed lines indicate the various polarizations of the linear and several rotating fields represented by the shapes shown below. The closed and open symbols denote the core switching and nonswitching events, respectively, at the corresponding field strengths and types. The purple (dark gray) and orange (light gray) solid lines indicate the analytical calculation of the threshold field strengths versus Δt for the up-to-down and down-to-up core switching, respectively. (b) Zoomed illustrations of XMCD contrast images at core regions before and after vortex-core switching driven by indicated types of applied fields.

observed, but with relatively high fields, because they were farther away from the corresponding ideal circular fields than the fields of $\Delta t = \pm 2.0$ ns. In the case of the linear fields, that is, $\Delta t = 0$, field strengths larger than $H_0 = 14.0$ Oe were required to switch either the upward or downward core

orientation. The threshold strength of the linear fields was higher than that of the CCW (CW) rotating fields (11.0 Oe) for the upward (downward) vortex-core switching. The actual threshold field strength for this linear field is the vector sum of both fields generated by the two orthogonal striplines at their interaction, that is, $\sqrt{2}H_0 = 19.8$ Oe. Our experimental results confirmed completely the analytical predictions of the upward (downward)-to-downward (upward) core switching at the given Δt values [the solid lines in Fig. 9(a)]. The analytical estimates also were confirmed to be in good agreement with simulation results obtained using the same rotating fields but smaller dimensions of Py disk.

VI. POSSIBLE MECHANISM OF VORTEX-CORE READOUT

An additional important observation drawn from the above experimental demonstration is that, similarly to the asymmetric switching response of the upward or downward core to the CCW or CW rotating field, there are large asymmetric vortex-core-gyration amplitudes, that is, resonantly excited versus nonexcited motion, depending on the relative rotation sense of the employed rotating fields with respect to a given core magnetization. Figure 10 shows the simulation results for the trajectories of the vortex-core gyrations of $p = +1$ and $p = -1$ in response to the pulse-type CCW and CW rotating fields. As consistent with the asymmetry of the switching behaviors evidenced in Fig. 9, the largest asymmetry in the vortex-core gyration amplitude between $p \cdot \text{sign}(\Delta t) = +1$ and -1 is obtained at $|\Delta t| = \frac{1}{2}\pi/\omega_D$. For the case of $p = +1$, only the CCW field ($\Delta t = +\frac{1}{2}\pi/\omega_D$) affects such a large-amplitude vortex-core gyration; the CW field ($\Delta t = -\frac{1}{2}\pi/\omega_D$) does not. A large-amplitude vortex-core gyration yields a large deviation of in-plane curling magnetization from the ground state vortex, which in turn gives rise to the corresponding
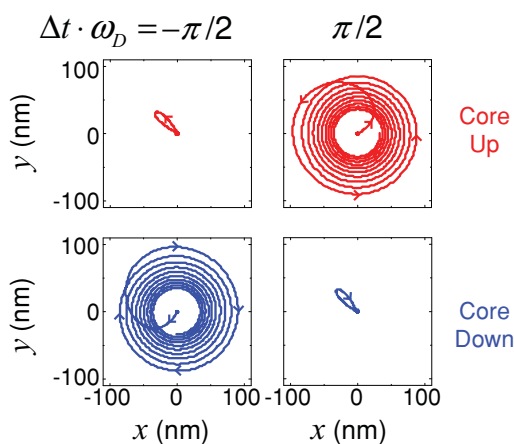

FIG. 10. (Color online) Asymmetry of vortex-core gyration amplitudes, represented by trajectories of upward and downward cores driven by pulse-type rotating fields with $\Delta t = \pm\frac{1}{2}\pi/\omega_D$, where $\omega_D/2\pi = 580$ MHz for Py disk of $R = 150$ nm and $L = 20$ nm. The field strength used, $H_0 = 150$ Oe, was weaker than the threshold field strength for vortex-core switching in the given disk dimensions.

difference in magnetization between the free and fixed vortex layers (e.g., in the spin value structure). Provided that the rotation sense of the fields applied as the input signal is known, readouts of either core orientation by reference to low and high tunneling magnetoresistance (TMR) through the magnetic tunneling junction (MTJ) is possible.[26] Thus, given a typical spin value structure that includes an MTJ, the change in TMR can be used as a readout means for detecting either vortex-core orientation.

VII. DISCUSSION

We want to emphasize the following significant points. We achieved polarization-selective vortex-core switching with either the CCW or CW rotating field even when using unipolar Gaussian-pulse currents, by changing just the sign of Δt, and that a significant reduction of the core-switching field was achieved simply by using the optimal pulse parameters $\sigma = 1/\omega_D$ and $\Delta t = \frac{1}{2}\pi/\omega_D$ rather than arbitrary ones.

The threshold field strength required for switching a vortex core of a given polarization varies significantly with the sign and magnitude of Δt. The threshold field strength for the linear field, when using only one electrode, is higher by a factor of almost two than that for the corresponding pulse-type rotating field when using two, crossed electrodes. When using the optimal pulse parameters in the above experiment, those values were 19.8 and 11.0 Oe, respectively. This large difference makes reliable cell selection possible without the half-selection problem that arises in conventional magnetic random access memory (MRAM). Such tailored pulse-type rotating fields which occur only at the selected intersection are a prerequisite for a reliable memory-bit selection and recording just by choosing two crossed electrodes at which intersection a given memory cell is positioned in the cross-point architecture, as we already demonstrated experimentally.[27]

It is also notable that the energy cost for switching in the Py sample used in the experiment is estimated to be 130 pJ. From our further analytical calculations considering only an ideal case, the energy cost was reduced dramatically with increasing thickness and decreasing diameter. Thus, for a case of the 100-nm diameter and 50-nm thicknesses, the energy cost roughly estimated based on the experimental power consumption and analytical calculations could be reduced down to 7 pJ. The value is still larger that, 1 pJ/bit, for the spin-transfer-torque MRAM, but is smaller than 120 pJ/bit for the conventional MRAM and smaller by three orders of magnitude than 30–120 nJ/bit for the flash memory.[28]

As for the storage density, smaller sizes of Py disks down to 100-nm diameter should be used in real devices so as to meet industrial needs. The roughly estimated storage density is $\sim$10 Gb/in.^{2} for the 100-nm diameter. A possible stacking of arrays of vortex-state disks in the vertical direction or new materials of much higher saturation magnetization would make the storage density higher.

VIII. CONCLUSIONS

The low-power-consumption switching of vortex cores in nanodisks by two orthogonal addressing electrodes

demonstrated in the present work is a promisingly robust mechanism for information writing operations in a vortex-state dot array. This, along with the proposed possible readout mechanism, has fruitful applications in nonvolatile information recording, writing, and readout operations. Thus, this work imparts further momentum to the realization of vortex random access memory based on the unique vortex structure and its novel dynamic properties.

We recently became aware of a recent work on "Optimal control of vortex-core polarity by resonant microwave pulses" which was published in *Nature Physics* (Ref. 29).

*Corresponding author: sangkoog@snu.ac.kr. S.K.K was on sabbatical research leave at the Center for X-Ray Optics, Materials Science Division Lawrence Berkeley National Laboratory.

[1] J. Raabe, R. Pulwey, R. Sattler, T. Schweinböck, J. Zweck, and D. Weiss, J. Appl. Phys. **88**, 4437 (2000).

[2] T. Shinjo, T. Okuno, R. Hassdorf, K. Shigeto, and T. Ono, Science **289**, 930 (2000).

[3] A. Wachowiak, J. Wiebe, M. Bode, O. Pietzsch, M. Morgenstern, and R. Wiesendanger, Science **298**, 577 (2002).

[4] R. P. Cowburn, Nat. Mater. **6**, 255 (2007).

[5] S.-K. Kim, K.-S. Lee, Y.-S. Yu, and Y.-S. Choi, Appl. Phys. Lett. **92**, 022509 (2008).

[6] B. Van Waeyenberge, A. Puzic, H. Stoll, K. W. Chou, T. Tyliszczak, R. Hertel, M. Fähnle, H. Brückl, K. Rott, G. Reiss, I. Neudecker, D. Weiss, C. H. Back, and G. Schütz, Nature (London) **444**, 461 (2006).

[7] Q. F. Xiao, J. Rudge, and B. C. Choi, Y. K. Hong, and G. Donohoe, Appl. Phys. Lett. **89**, 262507 (2006).

[8] R. Hertel, S. Gliga, M. Fähnle, and C. M. Schneider, Phys. Rev. Lett. **98**, 117201 (2007).

[9] K.-S. Lee, K. Y. Guslienko, J.-Y. Lee, and S.-K. Kim, Phys. Rev. B **76**, 174410 (2007).

[10] A. Vansteenkiste, K. W. Chou, M. Weigand, M. Curcic, V. Sackmann, H. Stoll, T. Tyliszczak, G. Woltersdorf, C. H. Back, G. Schütz, and B. Van Waeyenberge, Nat. Phys. **5**, 332 (2009).

[11] M. Curcic, B. Van Waeyenberge, A. Vansteenkiste, M. Weigand, V. Sackmann, H. Stoll, M. Fähnle, T. Tyliszczak, G. Woltersdorf, C. H. Back, and G. Schütz, Phys. Rev. Lett. **101**, 197204 (2008).

[12] K. Yamada, S. Kasai, Y. Nakatani, K. Kobayashi, H. Kohno, A. Thiaville, and T. Ono, Nat. Mater. **6**, 269 (2007).

[13] M. Weigand, B. Van Waeyenberge, A. Vansteenkiste, M. Curcic, V. Sackmann, H. Stoll, T. Tyliszczak, K. Kaznatcheev, D. Bertwistle, G. Woltersdorf, C. H. Back, and G. Schütz, Phys. Rev. Lett. **102**, 077201 (2009).

[14] Y. Liu, S. Gliga, R. Hertel, and C. M. Schneider, Appl. Phys. Lett. **91**, 112501 (2007).

[15] K. Yamada, S. Kasai, Y. Nakatani, K. Kobayashi, and T. Ono, Appl. Phys. Lett. **93**, 152502 (2008).

[16] K.Y. Guslienko, K.-S. Lee, and S.-K. Kim, Phys. Rev. Lett. **100**, 027203 (2008).

[17] S.-K. Kim, Y.-S. Choi, K.-S. Lee, K. Y. Guslienko, and D.-E. Jeong, Appl. Phys. Lett. **91**, 082506 (2007).

[18] K.-S Lee, S.-K. Kim, Y.-S. Yu Y.-S. Choi, K. Y. Guslienko, H. Jung, and P. Fischer, Phys. Rev. Lett. **101**, 267206 (2008).

[19] V. P. Kravchuk, Y. Gaididei, and D. D. Sheka, Phys. Rev. B **80**, 100405R (2009).

[20] K.-S. Lee and S.-K. Kim, Phys. Rev. B **78**, 014405 (2008).

[21] A. A. Thiele, Phys. Rev. Lett. **30**, 230 (1973); D. L. Huber, Phys. Rev. B **26**, 3758 (1982).

[22] K. Y. Guslienko, B. A. Ivanov, V. Novosad, Y. Otani, H. Shima, and K. Fukamichi, J. Appl. Phys. **91**, 8037 (2002); K. Y. Guslienko, X. F. Han, D. J. Keavney, R. Divan, and S. D. Bader, Phys. Rev. Lett. **96**, 067205 (2006).

[23] M. J. Donahue and D. G. Porter, *OOMMF User's Guide, Version 1.0* (NIST, Gaithersburg, MD, 1999).

[24] L. D. Landau and E. M. Lifshitz, Phys. Z. Sowjetunion **8**, 153 (1935); T. L. Gilbert, Phys. Rev. **100**, 1243A (1955).

[25] P. Fischer, D.-H. Kim, W. Chao, J. A. Liddle, E. H. Anderson, and D. T. Attwood, Mater. Today **9**, 26 (2006).

[26] N. Locatelli, V. V. Naletov, J. Grollier, G. de Loubens, V. Cros, C. Deranlot, C. Ulysse, G. Faini, O. Klein, and A. Fert, Appl. Phys. Lett. **98**, 062501 (2011).

[27] Y.-S. Yu, H. Jung, K.-S. Lee, P. Fischer, and S.-K. Kim, Appl. Phys. Lett. **98**, 052507 (2011).

[28] S. A. Wolf, A. Y. Chtchelkanova, and D. M. Treger, IBM J. Res. Dev. **50**, 101 (2006).

[29] B. Pigeau, G. de Loubens, O. Klein, A. Riegler, F. Lochner, G. Schmidt, and L. W. Molenkamp, Nat. Phys. **7**, 26 (2011).